Temperature Dependence of Cluster Ion Decomposition in a Quadrupole Ion Trap†

Edward R. Lovejoy*

NOAA Aeronomy Laboratory, 325 Broadway, Boulder, Colorado 80305-3337

Roberto Bianco

Department of Chemistry and Biochemistry, University of Colorado, Boulder, Colorado 80309-0215

Received: March 30, 2000; In Final Form: June 12, 2000

Rate coefficients for the thermal decomposition of $H^+(H_2O)_{3,4}$, $H^+(CH_3OH)_3$, $H^+(C_2H_5OH)_2$, $H^+(CH_3CN)_2$, $H^+((CH_3)_2CO)_2$, $NO_3^-(HNO_3)_{1,2}$, and Cl^-H_2O are measured as a function of temperature in a quadrupole ion trap over the pressure range 0.2−2 mTorr of He. The kinetics are in the low pressure limit and the decomposition activation energies are significantly less than the bond energies. The difference between the bond energy and the activation energy is reproduced by theory. The vibrational frequencies of the cluster ions necessary for the theoretical treatment of the dissociation rate constants are calculated *ab initio* at the HF/6-31G* level. This work demonstrates that cluster ion bond energies may be determined accurately from activation energies for dissociation at the low-pressure limit. The measurements also yield fundamental information about the intermolecular energy transfer between the helium buffer gas and the cluster ions.

Introduction

The thermochemistry of cluster ions is fundamental to the understanding of a variety of phenomena, such as homogeneous gas-phase nucleation, the solvation of ions in liquids, and atmospheric chemistry. Ion thermodynamics have been derived from a variety of measurements. Measurements of equilibrium constants as a function of temperature have provided a significant amount of thermodynamic information for cluster ions (see, e.g., ref 1). Bracketing techniques, in which the reactivity of an ion is measured with a set of compounds with known properties, e.g., proton affinity, gas-phase acidity, etc., also yield accurate thermodynamic data (see, e.g., ref 2). Bond energies are also derived from tandem mass spectrometric measurements of the threshold for collision induced dissociation (see, e.g., ref 3). Recently, the temperature dependence of the kinetics of ion dissociation induced by blackbody radiation in ion cyclotron resonance (ICR) traps has been exploited to derive thermodynamics of cluster ions and large biomolecular ions.[4] Schemes employing the radio frequency quadrupole ion trap to measure ion thermodynamics are just now being explored. Hart and McLuckey[5] and Colorado and Brodbelt[6] have shown that the thresholds for the decomposition of ions resonantly excited in an ion trap correlate with bond energies. Recently, Asano et al.[7] measured the temperature dependence of the rate constant for decomposition of ions derived from leucine enkephalin in an ion trap. They showed that the rate constant for decomposition was independent of the trapping voltage, confirming that the ion internal temperature is essentially equivalent to the temperature of the He buffer gas. They reported activation energies for the ion decomposition reactions that were statistically different from the zero pressure blackbody results from Schnier et al.[8] They postulated that the kinetics were not in the high-pressure limit in the quadrupole ion trap experiments. Butcher et al.[9] recently reported the Arrhenius parameters for the thermal dissociation of singly, doubly, and triply charged bradykinin ions in a quadrupole trap. They demonstrated that the kinetics were independent of the He bath gas pressure confirming that the kinetics were in the high pressure limit. In this case the activation energy corresponds closely to the bond energy. The Arrhenius parameters and product yields agree well with the results from blackbody induced radiative dissociation experiments.[8,10]

In the present study, the temperature dependencies of rate constants for decomposition of a variety of small cluster ions are measured in a quadrupole ion trap in the presence of He buffer gas. The dissociation kinetics are in the low pressure limit and the activation energies are significantly less than the bond energy. It is shown that the activation energies for decomposition are well predicted by theory, given the thermodynamics for ion decomposition. Hence, ion bond energies can be derived accurately from measurements of the low-pressure limit activation energies. These measurements also yield fundamental information about intermolecular energy transfer between He and the cluster ions.

Experimental Section

The apparatus used in the present study is similar to that described previously.[11] For the present study the ion trap was equipped with heaters to control the trap temperature between about 30 and 300 °C. The ion trap was housed in an aluminum box about 10% larger than the trap. The box consisted of two isolated and nested halves, each half was attached to an individual end cap of the ion trap. Cartridge heaters were embedded in each half of the box. Five small platinum resistance temperature detectors (RTD) encapsulated in ceramic were used to monitor the temperature of the ring electrode, each end cap, and the two halves of the aluminum box. The ring RTD was potted into a hole in the side of the ring electrode with ceramic epoxy. The end cap RTDs were clamped to the end caps close to the apertures on the exterior stainless steel surface. The temperatures of the end caps were maintained to ±1 K with

† Part of the special issue "C. Bradley Moore Festschrift."

10.1021/jp001216q CCC: $19.00
Published on Web 07/29/2000

temperature controllers reading the RTDs clamped to the aluminum box halves. The surface area of the interior of the aluminum box and the trap electrodes was significantly larger than the area of the apertures in the box and electrodes (approximately 50 times). Therefore, He atoms inside the trap had many collisions with the heated metal surfaces during their residence time in the trap, and the He in the trapping region was at the temperature of the trap electrodes. At steady state, the ring electrode was slightly warmer than the surface temperature of the end caps on the outside of the trap. The difference varied from about 1 °C at 50 °C to about 5 °C at 300 °C. The reaction temperature was taken as the average of the ring and end cap temperatures. The RTDs were accurate to 1 °C at the temperature of ice water and boiling water.

Cluster ions were generated in the external ion molecule reactor by adding reagent gases downstream of the filament electron source. High purity He (99.999%) was added directly to the trap chamber to control the chamber pressure. The pressure in the trap chamber due to the ion molecule reactor flow was typically less than 0.05 mTorr. The cluster ions were sampled from the end of the reactor through a Ni orifice (0.25 mm dia.) and focused into the ion trap with three electrostatic lenses. Ions were accumulated for 5 to 20 ms and isolated with a notched filtered noise field. The ions reacted for a variable delay time (20 to 10000 ms), and then were scanned out of the trap with a mass instability scan and axial modulation at 440 kHz. Product ions were also monitored. Typically, the signals from 10 trap-react-scan sequences were averaged for each delay time. The pseudo-first-order rate coefficient for ion decomposition was derived from the exponential decay of the ion signal versus trap residence time, and was measured as a function of the ion trap pressure from about 0.2 to 2 mTorr. The second-order decomposition rate coefficients were determined from the slope of the pseudo first-order rate constants versus He concentration. Second-order rate coefficients were measured as a function of trap temperature.

For the present trap configuration, the dimensionless trapping parameter q_z is given by[12]

$$q_z = \frac{0.048 V_{p-p}}{m} \tag{1}$$

where V_{p-p} is the peak to peak RF voltage on the ring electrode and m is the ion mass in amu. The fundamental oscillation frequency of a trapped ion scales with q_z, and ions are unstable in the axial direction (z) for $q_z > 0.908$. The influence of the trapping field on the internal energy of the cluster ions was examined by measuring the pseudo first-order rate coefficients for ion decomposition as a function of the trapping voltage (i.e., q_z). These measurements were performed at a fixed reaction temperature on the low end of the temperature range where the kinetics should be most sensitive to energy added by the trapping field.

The ion trap chamber pressure was measured with a capacitance manometer operating at 45 °C. The pressure in the trap was calculated from the measured chamber pressure with correction for thermal transpiration. Since the mean free path of He is significantly larger than the openings in the ion trap heater box, and the pressure is measured outside of the box, the pressure in the trap is given by[13]

$$p_{trap} = p_{man}\sqrt{\frac{T_{trap}}{T_{man}}} \tag{2}$$

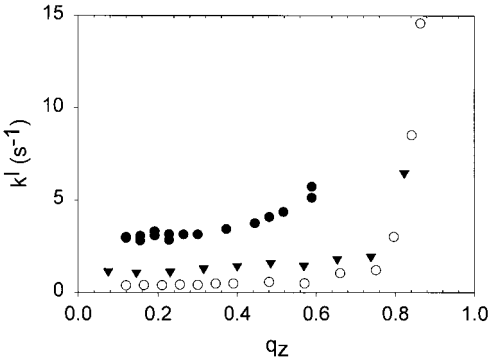

Figure 1. First-order decomposition rate coefficients as a function of the trapping parameter q_z. Solid circles are $H^+(H_2O)_4$ at 307 K in 1.56 mTorr of He. Open circles are $H^+((CH_3)_2CO)_2$ at 437 K in 1.24 mTorr of He. Filled triangles are $NO_3^-(HNO_3)_2$ at 310 K in 1.00 mTorr of He.

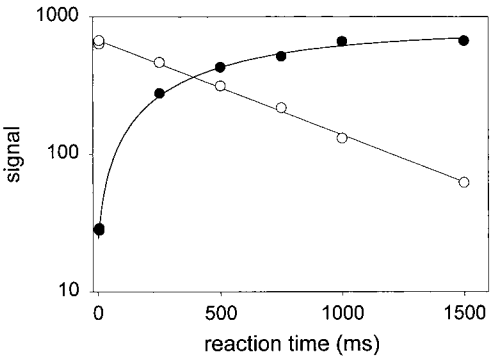

Figure 2. Both $H^+(H_2O)_3$ (open circles) and $H^+(H_2O)_2$ (filled circles) signals as a function of reaction time at 399 K in 1.91 mTorr of He. The lines are both calculated with a first-order decomposition rate coefficient of 1.6 s^{-1}.

where the subscripts "man" and "trap" refer to the manometer and the trap, respectively.

It follows that the concentration of He (molecules cm^{-3}) in the ion trap is given by

$$[He]_{trap} = \frac{9.66 \times 10^{18} p_{man}}{\sqrt{T_{trap} T_{man}}} \tag{3}$$

where the pressure is in Torr and the temperature is in Kelvin.

Results

The variations of the first-order rate coefficients for the decomposition of $H^+(H_2O)_4$, $H^+((CH_3)_2CO)_2$, and $NO_3^-(HNO_3)_2$ as a function of the trapping parameter q_z are shown in Figure 1. As an example of the activation energy measurements, data for the reaction $H^+(H_2O)_3 \rightarrow H^+(H_2O)_2 + H_2O$ are presented. The variation of the signals of $H^+(H_2O)_3$ and $H^+(H_2O)_2$ as a function of reaction time at 399 K in 1.9 mTorr of He are shown in Figure 2. The pseudo-first-order rate coefficients derived from the slopes of the $H^+(H_2O)_3$ decays are plotted as a function of the He concentration for a range of temperatures in Figure 3. The slopes yield the second-order low-pressure limit decomposition rate coefficients. Typically, the standard deviations of the second-order rate coefficients were less than 5% of the rate constants. The measured temperature dependencies of the low-pressure limit rate coefficients for decomposition of the cluster ions are presented in Figure 4.

Collision efficiencies, defined as the ratios of measured rate coefficients to the calculated strong collision rate coefficients,

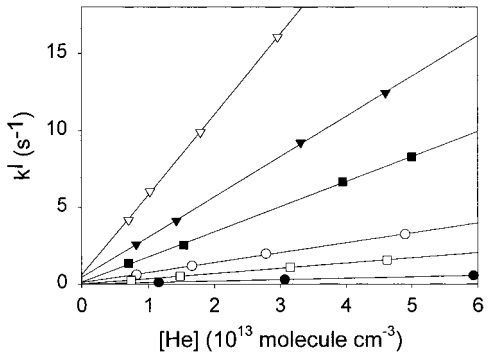

Figure 3. First-order decomposition rate constants for $H^+(H_2O)_3$ as a function of the He concentration in the trap: (filled circles) 369 K, (open squares) 399 K, (open circles) 415 K, (filled squares) 445 K, (filled triangles) 464 K, and (open triangles) 491 K.

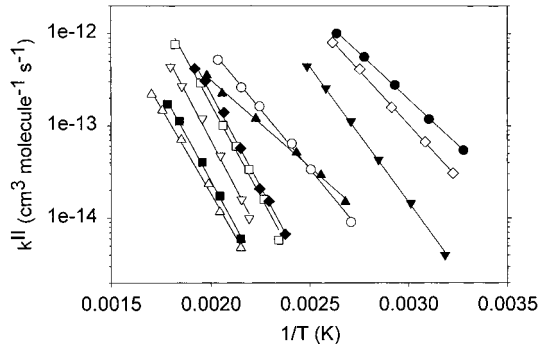

Figure 4. Temperature dependence of the second-order low-pressure limit decomposition rate coefficients: (solid circles) $H^+(H_2O)_4$, (open circles) $H^+(H_2O)_3$, (inverted solid triangles) $H^+(CH_3OH)_3$, (inverted open triangles) $H^+(C_2H_5OH)_2$, (solid squares) $H^+(CH_3CN)_2$, (open squares) $H^+((CH_3)_2CO)_2$ with $q_z = 0.12$, (solid diamonds) $H^+((CH_3)_2CO)_2$; with $q_z = 0.24$, (open diamonds) $NO_3^-(HNO_3)_2$, (solid triangles) Cl^-H_2O, and (open triangles) $NO_3^-HNO_3$.

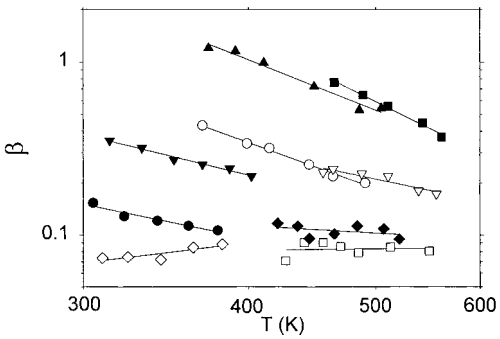

Figure 5. Collision efficiency as a function of temperature for a harmonic treatment of the low-frequency torsional modes. Symbols are the same as in Figure 4. Lines are fits to the equation $\beta \propto T^{-n}$.

are presented in Figures 5 and 6 as a function of the temperature. The strong collision rate coefficient is an upper limit to the decomposition rate coefficient in the low-pressure limit, and is derived by assuming that collisions transfer sufficient energy to maintain a Boltzmann distribution of energy in the reactant. Strong collision rate coefficients were calculated with Troe's approach[14,15,16] outlined in Appendix A. The following assumptions and procedures were used in the strong collision calculations (1). The number of Morse oscillators used in the calculation of the anharmonicity correction was set equal to the number of oscillators that disappeared in the dissociation. (2) The rotations were assumed to be fully activated and able to contribute to the dissociation. (3) Low frequency (<300 cm^{-1}) torsional modes were treated both as harmonic oscillators (Figure 5) and

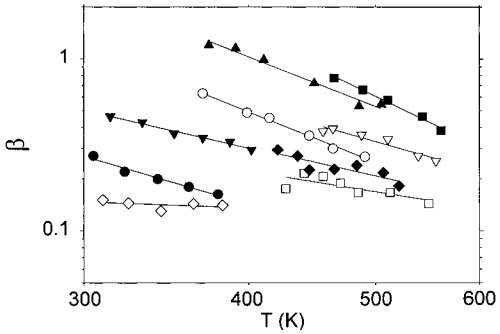

Figure 6. Collision efficiency as a function of temperature for a free rotor treatment of the low-frequency torsional modes. Symbols are the same as in Figure 4. Lines are fits to the equation $\beta \propto T^{-n}$.

as free internal rotors (Figure 6). Cluster ion vibrational frequencies were calculated at the HF/6-31G* level using the GAMESS program[17] and were scaled by the factor 0.89 as recommended by Scott and Radom[18] for thermodynamic calculations using HF/6-31G* frequencies. The cluster ion structures are shown in Figure 7. Detailed information on structures, energies and frequencies is included as Supporting Information. The optimized structures of the cluster ions are consistent with previous calculations.[19]

Low-pressure limit activation energies were derived from fits of the data in Figure 4 to the expression

$$E_a = -k\frac{\partial \ln k_o^{II}}{\partial(1/T)} \tag{4}$$

by minimizing the sum of the squares of the residuals weighted by the reciprocal of the variance. k_o^{II} is the second-order low-pressure limit rate coefficient for decomposition, and k is the Boltzmann constant. The experimental parameters and measured activation energies are listed in Table 1. The quoted errors for the activation energies are based on 10% uncertainty in the rate coefficients.

Discussion

For each cluster ion studied, the first-order decomposition rate coefficient increased linearly with the concentration of He in the ion trap (see e.g. Figure 3), thus verifying that the decomposition kinetics were in the low-pressure limit. For all the ions, except $H^+(H_2O)_4$ and Cl^-H_2O, the intercepts were statistically significant (greater than twice the standard deviation) and increased with temperature. The intercepts were typically less than 10% of the largest first-order rate coefficient measured, except for $H^+(C_2H_5OH)_2$ and $H^+(CH_3CN)_2$, for which the intercepts were about 20% of the largest rate coefficients. Blackbody radiation induced dissociation is probably too slow to explain the intercepts. Tholmann et al.[20] report a zero pressure first-order decomposition rate coefficient for $H^+(H_2O)_4$ of about 5×10^{-3} s^{-1} at room temperature. This is significantly smaller than the intercepts measured in the present work. Intercepts as high as 1 and 2 s^{-1} were observed for $H^+(CH_3CN)_2$ at 561 K and $H^+(C_2H_5OH)_2$ at 556 K, respectively.

The intercepts could be attributed to reaction channels that are independent of pressure. For example, in the $H^+(C_2H_5OH)_2$ studies a significant yield of mass 75 product ion (10−20% yield at the highest pressures and temperatures) was observed. This could be explained by the reaction

$$H^+(C_2H_5OH)_2 \rightarrow H^+(C_2H_5)_2O + H_2O \tag{5}$$

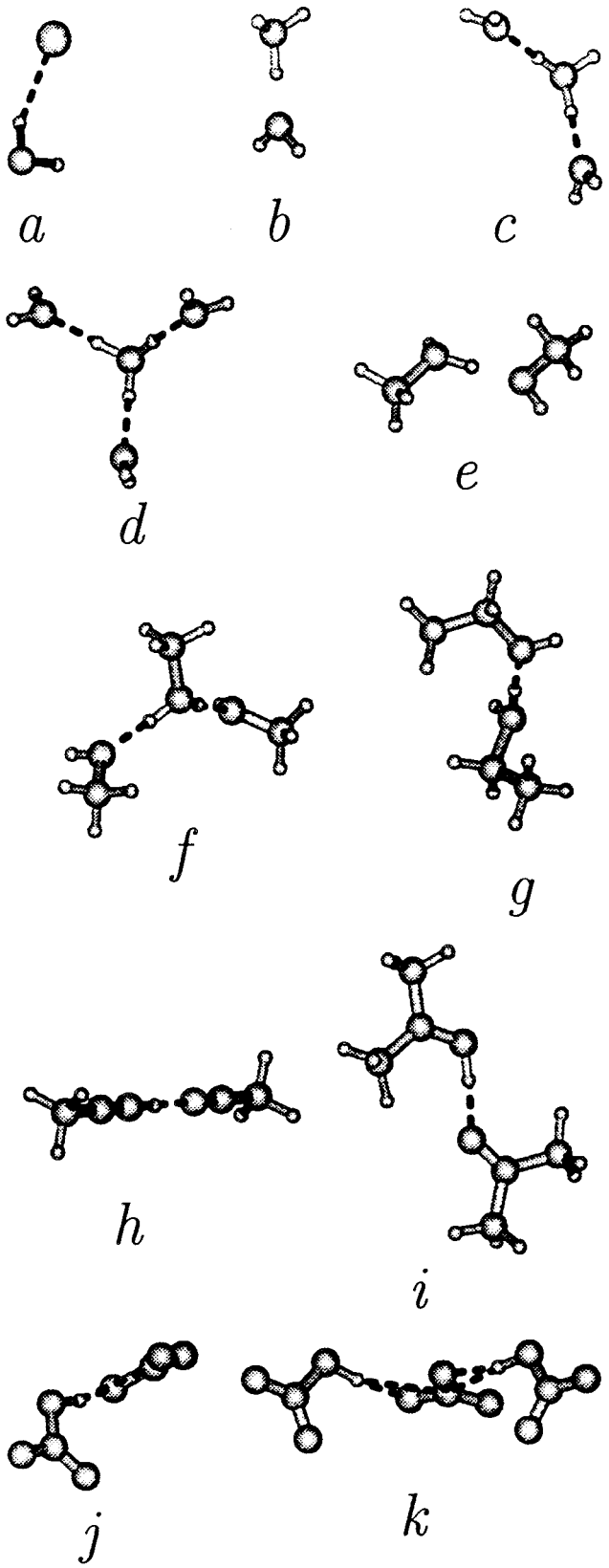

Figure 7. HF/6-31G* optimized structures for the following complexes: (a) Cl^-H_2O. (b) $H^+(H_2O)_2$. (c) $H^+(H_2O)_3$. (d) $H^+(H_2O)_4$. (e) $H^+(CH_3OH)_2$. (f) $H^+(CH_3OH)_3$. (g) $H^+(CH_3CH_2OH)_2$. (h) $H^+(CH_3CN)_2$. (i) $H^+((CH_3)_2CO)_2$. (j) $NO_3^-HNO_3$. (k) $NO_3^-(HNO_3)_2$.

Similar reactions are observed for CH_3OH [21] and higher alcohols.[22] Reaction 5 is about 12 kcal mol^{-1} endothermic and probably has a barrier and a highly constrained transition state associated with significant molecular rearrangement. A tight transition state could make the unimolecular reaction rate limiting and the kinetics independent of pressure.

TABLE 1: Literature Reaction Enthalpies and Bond Energies

reaction	T^a(K)	ΔH^o_T[b] (kcal mol^{-1})	ref	E^c_o (kcal mol^{-1})
$H^+(H_2O)_4 \rightarrow$	400	17.6(1.0)	32	17.6, 17.4
$H^+(H_2O)_3 + H_2O$	395	17.5(1.8)	33	17.5, 17.3
	298	16.7(1.3)	34	16.5, 16.3
	0	17.5(0.5)	35	17.5, 17.5
	440	16.0(1.5)	36	16.1, 15.8
	0	16.3(0.9)	37	16.3, 16.3
	385	17.9	38	17.9, 17.6
$H^+(H_2O)_3 \rightarrow$	525	19.0(1.0)	32	19.2, 18.6
$H^+(H_2O)_2 + H_2O$	525	19.5	33	19.7, 19.1
	298	20.5(1.3)	34	20.1, 19.8
	0	21.9(1.2)	35	21.9, 21.9
	540	21.0	36	21.2, 20.6
	0	20.1(2.3)	37	20.1, 20.1
	510	20.2	39	20.3, 19.8
$H^+(CH_3OH)_3 \rightarrow$	430	21.3(2.1)	40	22.8, 21.6
$H^+(CH_3OH)_2 + CH_3OH$				
$H^+(C_2H_5OH)_2 \rightarrow$	630	31.3	41	32.2, 31.5
$H^+C_2H_5OH + C_2H_5OH$	630	31.7	42	32.6, 31.9
$H^+(CH_3CN)_2 \rightarrow$	630	30.2(1.0)	43	31.4, 30.8
$H^+CH_3CN + CH_3CN$				
$H^+((CH_3)_2CO)_2 \rightarrow$	620	30.1(1.0)	44	31.4, 30.8
$H^+(CH_3)_2CO + (CH_3)_2CO$	650	32.1	41	33.5, 32.9
	630	29.6	39	31.0, 30.4
$NO_3^-HNO_3 \rightarrow$	367	>21.8	45	>22.3, >21.4
$NO_3^- + HNO_3$				
$NO_3^-(HNO_3)_2 \rightarrow$	350	18.3(1.0)	45	19.0, 19.2
$NO_3^-HNO_3 + HNO_3$	365	17.7(0.2)	46	18.4, 18.6
	345	16.0(0.8)	47	16.6, 16.8
$Cl^-H_2O \rightarrow Cl^- + H_2O$	370	14.7(0.6)	48	12.9, 12.9
	410	13.1	49	11.2, 11.2
	495	14.9(0.1)	50	12.8, 12.8
	375	14.9	51	13.1, 13.1
	300	14.4	52	12.8, 12.8

[a] Median temperature. [b] Errors are in parentheses. [c] Calculated with eq A17. The first value is for a harmonic treatment of low frequency torsional vibrations, and the second is for a free rotor treatment.

The intercepts in the k^1 vs [He] data could also be attributed to decomposition induced by species from the ion source and/or from ion trap outgassing. Large molecules present in the ion source may be very efficient activation agents and, despite low partial pressures in the ion trap, could lead to a measurable loss. The loss would be independent of the ion trap pressure, since the flow from the ion source is constant. This loss would also have a strong temperature dependence similar to the He mediated decomposition. Reactions with species from ion trap outgassing would have even stronger temperature dependencies because both the concentration of the gas and the rate coefficients would increase with temperature. In the $H^+(CH_3CN)_2$ and $H^+(C_2H_5OH)_2$ experiments, partial pressures of CH_3CN and C_2H_5OH in the ion trap were less than 10^{-7} Torr. Therefore, the collision efficiencies of CH_3CN and C_2H_5OH would have to be at least 10^3 times larger than the He efficiency to account for the intercepts. However, this is very unlikely (see, e.g., ref 23).

Another possible explanation for the intercepts is a temperature dependent physical loss from the trap. This loss could be mediated by impurities from outgassing. This is unlikely because the intercepts varied significantly among the different ions at the same trap temperature. Physical loss from the trap mediated by the helium gas is slow for stable ions (<0.02 s^{-1}).

The apparent product ion yield usually increased as the pressure in the trap increased. This effect was most pronounced

TABLE 2: Measurement Conditions, Activation Energies, and Derived Parameters

ion	q_z	E_o lit[a] (kcal mol^{-1})	E_a (kcal mol^{-1})[b]	T (K)[c]	$U_v(T)$ (kcal mol^{-1})	n	a	E_o predicted (kcal mol^{-1})[d]
$H^+(H_2O)_4$	0.16	17.1,16.9	9.2(0.4)	342	7.1,6.4	1.6,2.2	1.2,1.9	17.1,16.8
$H^+(H_2O)_3$	0.21	20.4,20.0	11.9(0.3)	430	6.5,5.8	2.8,3.0	2.3,2.7	19.4,19.2
$H^+(CH_3OH)_3$	0.12	22.8,21.6	13.5(0.3)	358	8.2,7.1	1.9,1.8	1.5,1.4	22.5,21.9
$H^+(C_2H_5OH)_2$	0.18	32.4,31.7	19.0(0.5)	506	12.3,11.0	1.6,2.2	1.1,1.7	32.5,31.8
$H^+(CH_3CN)_2$	0.17	31.4,30.8	18.2(0.6)	513	9.7,9.2	3.8,3.7	3.4,3.3	29.1,29.2
$H^+((CH_3)_2CO)_2$	0.12	32.0,31.4	18.4(0.4)	488	14.3,12.4	−0.1,1.2	−0.7,0.6	33.9,32.5
$H^+((CH_3)_2CO)_2$	0.24	32.0,31.4	18.4(0.5)	471	13.5,11.6	0.5,1.7	0.1,1.5	32.4,31.4
$NO_3^-HNO_3$	0.11	>22.3, >21.4	17.2(0.5)	526	8.3,6.9			26.8,26.0
$NO_3^-(HNO_3)_2$	0.08	18.0,18.2	10.7(0.4)	346	8.2,7.5	−0.9,0.3	−1.3,0.0	19.7,19.4
Cl^-H_2O	0.21	12.6,12.6	8.7(0.3)	439	1.5,1.5	3.0,3.0	2.8,2.8	11.2,11.8

[a] Average of the literature values listed in Table 1. The first value is for the harmonic treatment of the torsional vibrations and the second is for the free rotor treatment (see text). [b] Measured activation energy. Errors are in parentheses. [c] Median temperature. [d] Bond energy predicted with equation (A16) using average a values of 1.2 and 1.8 for the harmonic and free rotor treatments, respectively.

for $H^+((CH_3)_2CO)_2$. The $H^+(CH_3)_2CO$ yields were greater than one over the whole pressure range (0.2−2.0 mTorr), with a maximum yield of about 7 at 2 mTorr. The absolute $H^+(CH_3)_2CO$ signals increased with pressure, and the $H^+((CH_3)_2CO)_2$ signals were relatively independent of pressure for the same accumulation times. The pressure dependent signal discrimination is probably due to decomposition of $H^+((CH_3)_2CO)_2$ as q_z is rapidly increased during the mass scan.

The kinetics for all of the ions were measured at low q_z (<0.25) where the decomposition rate constants were only weak functions of the trapping parameter (see Figure 1). Full temperature dependencies were measured for the protonated acetone dimer at both $q_z = 0.12$ and 0.24. The measured activation energy was independent (<5% difference) of q_z over this range, supporting the assumption that at low q_z the trapping field does not significantly perturb the internal energy of the ions. At higher q_z values (>0.6) the ion decomposition rate coefficients increased significantly, consistent with internal energy enhancement by the trapping field.

The largest uncertainty in the calculation of the strong collision rate coefficient is due to the uncertainty in the experimental threshold energy, E_o. The literature bond enthalpies for the clusters examined in this work are typically uncertain by about 1 kcal mol^{-1} (see Table 1) which translates to uncertainties in the strong collision rate coefficient and collision efficiencies of up to a factor of 5. The calculated strong collision rate coefficients also depend on the treatment of the low-frequency torsional modes. The strong collision rate coefficients decrease by up to a factor of 2 when the low frequency torsional modes are treated as free rotors (cf. Figures 5 and 6). The strong collision rate coefficients are less sensitive to the absolute values of the vibrational frequencies. For example, simultaneously decreasing all the vibrational frequencies for $H^+(H_2O)_4$ by 10% increases the calculated rate coefficients by about 20% with negligible change in the temperature dependence. The strong collision rate coefficients are a weak function of the number of vibrations that are treated as Morse oscillators. For example, varying the number of Morse oscillators from 0 to 6 increases the $H^+(H_2O)_4$ rate coefficients by only 10% with no change in the strong collision activation energy.

The temperature dependencies of the collision efficiencies were fit to the expression $\beta \propto T^{-n}$. The fits are shown as solid lines in Figures 5 and 6. Values of the temperature exponents n are listed in Table 2. The temperature exponents range from about 4 to −1 with average values of 1.6 and 2.1 for the harmonic and free rotor treatments of the torsional modes, respectively. Comparison of the average n values with the theoretical expressions for the collision frequency (eqs A13 and A14) suggest that the average energy transferred in all collisions

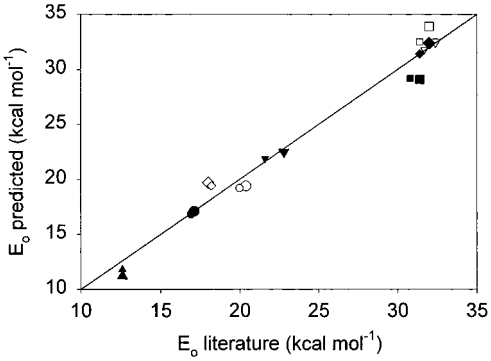

Figure 8. Predicted bond energy as a function of the average literature bond energy. The symbols are the same as in Figure 4. Large and small symbols refer to the harmonic and free rotor treatments of the torsional vibrations, respectively.

scales roughly as T^{-1}, and the average energy transferred in down collisions (energy of ion decreases in the collision) is relatively independent of temperature. Brown et al.[24] report that the average energy transferred in down collisions for ethyl acetate/He scales as $T^{-0.2 \pm 0.1}$. They also report collision efficiencies of 0.02 at 837 K and 0.2 at 340 K, yielding a collision efficiency temperature exponent n of 2.6. These numbers are consistent with the results of the present work. Krongauz and Rabinovitch[25] report collision efficiencies for cyclopropane/He that decrease from 0.08 at 773 K to 0.01 at 1175 K giving a temperature coefficient of n of 5.5. This is a much stronger temperature dependence than observed in the present work.

Values of a defined by eq A16, $E_a \cong E_o - U_v - akT$, were also calculated from the data. The vibrational energies and a values are listed in Table 2. Average values of a were 1.2 and 1.8 for harmonic and free rotor treatments, respectively. Predicted values of the bond energies from eq A16 using the average a values are also listed in Table 2 and plotted versus the literature energies in Figure 8. For all of the clusters except $H^+(CH_3CN)_2$, the predicted bond energies are within the range of the literature values. The average of the absolute values of the differences between the literature and the predicted bond energies are 1.1 and 0.7 kcal mol^{-1} for the harmonic and free rotor treatments, respectively.

There is a strong correlation between the bond energy E_o and the collision efficiency temperature exponent n. For example, decreasing the bond energy by 1 kcal mol^{-1} decreases n by about 1 unit. The large range of temperature exponents observed for the cluster ions could be related to the uncertainty in the bond energies. There is a general trend apparent in Figures 5 and 6 where the clusters with the largest temperature exponents

(e.g., Cl^-H_2O and $H^+(CH_3CN)_2$) have unusually high collision efficiencies, perhaps suggesting that E_o may be too large for these species. Decreasing E_o decreases the temperature exponent and increases the strong collision rate coefficient, thereby decreasing the collision efficiency.

The bond energy of $NO_3^-HNO_3$ is not well established. Davidson et al.[26] report $\Delta H^o_{367K} > 21.8$ kcal mol^{-1} based on equilibrium measurements. They also derived an absolute value of 26 kcal mol^{-1} for the enthalpy of the $NO_3^-HNO_3 \rightarrow NO_3^- + HNO_3$ reaction based on the following thermochemical cycle

$$NO_3^-HNO_3 + HBr \rightleftarrows NO_3^-HBr + HNO_3 \quad (6)$$

$$NO_3^-HBr + HBr \rightleftarrows Br^-HBr + HNO_3 \quad (7)$$

$$Br^- + HNO_3 \rightleftarrows NO_3^- + HBr \quad (8)$$

$$Br^-HBr \rightleftarrows Br^- + HBr \quad (9)$$

$$\textbf{net}: \; NO_3^-HNO_3 \rightleftarrows NO_3^- + HNO_3 \quad (10)$$

by using their results for reactions 6−8 and an estimate for the Br^-HBr bond energy.[27] Their result for the $NO_3^-HNO_3 \rightarrow NO_3^- + HNO_3$ reaction is consistent with the value $\Delta H^o_{300K} = 26.4 \pm 1.0$ kcal mol^{-1} derived in the present study.

Summary

Measurements of the temperature dependence of the thermal decomposition of a variety of cluster ions in a quadrupole ion trap yield low-pressure limit decomposition activation energies. It is shown that the cluster ion bond energy E_o is related simply to the decomposition activation energy E_a and the vibrational energy U_v by

$$E_o = E_a + U_v + akT \quad (11)$$

Equation 11 reproduces the literature bond energies to better than 1 kcal mol^{-1}, which is comparable to the uncertainty in the literature energies. This work demonstrates that combining measured activation energies and *ab initio* vibrational frequencies is a viable method for deriving accurate cluster ion bond energies.

Appendix A: Unimolecular Decomposition at the Low-Pressure Limit

The unimolecular reaction A + M → B + C + M may be represented by activation, deactivation, and dissociation steps (see e.g., ref 28)

$$A + M \rightarrow A^*(E,J) + M; \quad k_1(E,J) \quad (A1)$$

$$A^*(E,J) + M \rightarrow A + M; \quad k_{-1}(E,J) \quad (A2)$$

$$A^*(E,J) \rightarrow B + C; \quad k_2(E,J) \quad (A3)$$

Where A*(*E*,*J*) is a molecule with energy *E* above the dissociation threshold ($E > E_o$) and angular momentum *J*. For A* in steady state, the rate coefficient for unimolecular decomposition of A is

$$k_{uni}(E,J) = \frac{k_1(E,J)k_2(E,J)[M]}{k_{-1}(E,J)[M] + k_2(E,J)} \quad (A4)$$

$k_{-1}(E,J)$ is the rate coefficient for deactivating A*(*E*,*J*) below the dissociation threshold, and is usually written as the product βZ, where *Z* is the rate coefficient for collisions between A* and M, and β is a collision efficiency. When each collision deactivates A*, the energy transfer is in the strong collision limit and $\beta = 1$. The ratio of the activation and deactivation rate constants is related to the fractional equilibrium population of state (*E*,*J*) by detailed balance

$$\frac{k_1(E,J)}{k_{-1}(E,J)} = p(E,J) \quad (A5)$$

Equation A4 shows that the unimolecular rate coefficient is a function of [M] and is therefore pressure dependent. In the low-pressure limit ([M] → 0) the dissociation kinetics are dictated by the rate of activation,

$$k_{uni}(E,J) = k_1(E,J)[M] = \beta Z p(E,J)[M] \quad (A6)$$

In the high-pressure limit ([M] → ∞), the energy transfer is much faster than the unimolecular decomposition, and the kinetics are limited by the decomposition of the excited molecule

$$k_{uni}(E,J) = \frac{k_1(E,J)k_2(E,J)}{k_{-1}(E,J)} = k_2(E,J)p(E,J) \quad (A7)$$

Thermal rate coefficients are obtained by averaging over energy and angular momentum

$$k_{uni}(T) = \int_{E_o}^{\infty} \sum_{J=0}^{\infty} k_{uni}(E,J)\mathrm{d}E \quad (A8)$$

The thermal unimolecular rate coefficient at the low pressure limit is usually written as the product of a weak collision efficiency β_c and a strong collision rate coefficient k_o^{sc}

$$k_o = \beta_c k_o^{sc} \quad (A9)$$

The strong collision rate coefficient is derived by combining eqs A6 and A8 ($\beta_c = 1$ in the strong collision regime)

$$k_o^{sc} = [M]Z \int_{E_o}^{\infty} \sum_{J=0}^{\infty} p(E,J)\mathrm{d}E \quad (A10)$$

For the simplest case of a nonrotating molecule consisting of harmonic oscillators, and with a density of vibrational states near threshold that is independent of energy, the low-pressure limit strong collision rate coefficient is

$$k_o^{sc} \cong [M]Z \frac{\rho_{vib,h}(E_o)kT}{Q_{vib}} \exp\left(\frac{-E_o}{kT}\right) \quad (A11)$$

where $\rho_{vib,h}(E_o)$ is the density of vibrational states at the dissociation threshold and Q_{vib} is the vibrational partition function. Troe[14,15,16] introduces factors to correct for the various approximations implicit in eq A11, and writes the strong collision rate coefficient as a product of the first order estimate and the correction factors

$$k_o^{sc} \cong [M]Z \frac{\rho_{vib,h}(E_o)kT}{Q_{vib}} \exp\left(\frac{-E_o}{kT}\right) F_{anh}F_E F_{rot}F_{rot\,int}F_{corr} \quad (A12)$$

The ion molecule collision rate coefficient *Z* is calculated with the Su and Chesnavich[29] parametrization. F_{anh} corrects the density of states for anharmonicity. F_E is a correction factor for the energy dependence of the density of states. F_{rot} and $F_{rot\,int}$

account for the influence of external and internal rotations on the density of states and the partition function, and F_{corr} is a correction term that accounts for coupling between the other terms. In the present work it is assumed that $F_{corr} = 1$.

Troe[14] solved the master equation for energy transfer on the basis of an exponential model for the energy transfer probabilities and derived the following expression for the collision efficiency

$$\frac{\beta}{1-\sqrt{\beta}} \approx \frac{-\langle \Delta E \rangle}{F_E kT} \tag{A13}$$

where $\langle \Delta E \rangle$ is the average energy transferred in all collisions. Equation A13 obtains in the weak collision limit $-\langle \Delta E \rangle \ll F_E kT$ for an exponential model of the energy transfer probabilities. This expression also appears to be a good approximation for a variety of other functional forms for the energy transfer probabilities. Tardy and Rabinovitch[30] express the weak collision efficiency as a function of the average energy transferred in down collisions, $\langle E \rangle_d$

$$\beta = \frac{\langle \Delta E \rangle_d^2}{(kT)^2 I} \tag{A14}$$

where $I \sim 1 + 2skT/E_o$. s is the number of classical oscillators.

Troe[14] presents an approximate equation that relates the weak collision activation energy E_a to the average internal energy $U_{v,r}$ and the dissociation threshold E_o

$$E_a \cong E_o - U_{v,r} + 0.5kT \tag{A15}$$

where it is assumed that the external rotations contribute fully to the dissociation, and the collision efficiency scales as T^{-1} (eq A13). $U_{v,r}$ is the average energy of the vibrations and rotations assuming a Boltzmann distribution. Noting that the average energy of the three free external rotations is about $1.5kT$, and generalizing to a collision efficiency that scales as T^{-a}, the activation energy is given approximately by

$$E_a \cong E_o - U_v - akT \tag{A16}$$

where U_v is the average vibrational energy of the dissociating species assuming a Boltzmann distribution of energy.

Dissociation thresholds E_o were derived from the literature bond enthalpies with the following expression

$$E_o = \Delta H_{0K} = \Delta H_T - \int_{0K}^{T} C_p(T)\mathrm{d}T \tag{A17}$$

Heat capacities were calculated with the *ab initio* vibrational frequencies using standard formulas (see, e.g., ref 31).

Acknowledgment. This paper is dedicated to Brad Moore on the occasion of his 60th birthday. E.R.L. is grateful to Carl Howard for useful discussions, and to Rob Wilson for technical support. R.B. thanks the NOAA Geophysical Fluid Dynamics Laboratory, Princeton, NJ, for a generous grant of computer time. This work was supported in part by NOAA's Global and Climate Change Program.

Supporting Information Available: Structures, energies, moments of inertia, and vibrational frequencies for cluster ions and ligands calculated at the HF/6-31G* level. This material is available free of charge via the Internet at http://pubs.acs.org.

References and Notes

(1) Kebarle, P. *Annu. Rev. Phys. Chem.* **1977**, *28*, 445.
(2) Yamdagni, R.; Kebarle, P. *J. Am. Chem. Soc.* **1976**, *98*, 1320.
(3) Dalleska, N. F.; Honma, K.; Armentrout, P. B. *J. Am. Chem. Soc.* **1993**, *115*, 12125.
(4) Dunbar, R. C.; McMahon, T. B. *Science* **1998**, *279*, 194. Price, W. D.; Schnier, P. D.; Williams, E. R. *J. Phys. Chem. B* **1997**, *101*, 664.
(5) Hart, K. J.; McLuckey, S. A. *J. Am. Soc. Mass Spectrom.* **1994**, *5*, 250.
(6) Colorado, A.; Brodbelt, J. *J. Am. Soc. Mass Spectrom.* **1996**, *7*, 1116.
(7) Asano, K. G.; Goeringer, D. E.; McLuckey, S. A. *Int. J. Mass Spectrom.* **1999**, *185*, 207.
(8) Schnier, P. D.; Price, W. D.; Jockusch, R. A.; Williams, E. R. *J. Am. Chem. Soc.* **1996**, *118*, 7178.
(9) Butcher, D. J.; Asano, K. G.; Goeringer, D. E.; McLuckey, S. A. *J. Phys. Chem. A* **1999**, *103*, 8664.
(10) Price, W. D.; Schnier, P. D.; Williams, E. R. *Anal. Chem.* **1996**, *68*, 859.
(11) Lovejoy, E. R.; Wilson, R. *J. Phys. Chem.* **1998**, *102*, 2309.
(12) *Practical Aspects of Ion Trap Mass Spectrometry*; March, R. E., Todd, F. J. F., Eds.; CRC: Boca Raton, 1995; Vol. I.
(13) Poulter, K. F.; Rodgers, M.-J.; Nash, P. J.; Thompson, T. J.; Perkin, M. P.; *Vacuum* **1983**, *33*, 311.
(14) Troe, J. *J. Chem. Phys.* **1977**, *66*, 4745.
(15) Troe, J. *J. Chem. Phys.* **1977**, *66*, 4758.
(16) Troe, J. *J. Phys. Chem.* **1979**, *83*, 114.
(17) Schmidt, M. W.; Baldridge, K. K.; Boatz, J. A.; Elbert, S. T.; Gordon, M. S.; Jensen, J. H.; Koseki, S.; Matsunaga, N.; Nguyen, K. A.; Su, S. J.; Windus, T. L.; Dupuis, M.; Montgomery, J. A. *J. Comput. Chem.* **1993**, *14*, 1347.
(18) Scott, A. P.; Radom, L. *J. Phys. Chem.* **1996**, *100*, 16502.
(19) (a) $H^+ \cdot (H_2O)_{3,4}$: Novakovskaya, Y. V.; Stepanov, N. F. *Int. J. Quantum Chem.* **1997**, *61*, 981. Plummer, P. L. M. *J. Phys. Chem. B* **1997**, *101*, 6251. Wei, D.; Salahub, D. R. *J. Chem. Phys.* **1994**, *101*, 7633. Lee, E. P. F.; Dyke, J. M. *Mol. Phys.* **1991**, *73*, 375. Lee, E. P. F.; Dyke, J. M.; Wilders, A. E.; Watts, P. *Mol. Phys.* **1990**, *71*, 207. Deakyne, C. A.; Meotner, M.; Campbell, C. L.; Hughes, M. G.; Murphy, S. P. *J. Chem. Phys.* **1986**, *84*, 4958. Scheiner, S. *J. Am. Chem. Soc.* **1981**, *103*, 315. Ojamae, L.; Shavitt, I.; Singer, S. J. *Int. J. Quantum Chem., Quantum Chem. Symp.* **1995**, *29*, 657. Cheng, H. P. J. Phys. Chem. A **1998**, *102*, 6201. Wang, Y. S.; Jiang, J. C.; Cheng, C. L.; Lin, S. H.; Lee, Y. T.; Chang, H. C. *J. Chem. Phys.* **1997**, *107*, 9695. Lee, E. P. F.; Dyke, J. M. *Mol. Phys.* **1991**, *73*, 375. Mestdagh, J. M.; Binet, A.; Sublemontier, O. *J. Phys. Chem.* **1989**, *93*, 8300. Yeh, L. I.; Okumura, M.; Myers, J. D.; Price, J. M.; Lee, Y. T. *J. Chem. Phys.* **1989**, *91*, 7319. Choi, J. Y.; Davidson, E. R.; Lee, I. *J. Comput. Chem.* **1989**, *10*, 163. (b) $H^+[(CH_3)_2CO]_2$: Lee, E. P. F.; Dyke, J. M. *J. Chem. Soc., Faraday Trans.* **1992**, *88*, 2111. Hiraoka, K.; Takimoto, H.; Yamabe, S. *J. Phys. Chem.* **1986**, *90*, 5910. Aviyente, V.; Vernali, T. *J. Mol. Struct.* (*Theochem*) **1992**, *96*, 285. (c) $H^+(CH_3CN)_{1,2}$: Meot-ner, M.; Sieck, L. W.; Koretke, K. K.; Deakyne, C. A. *J. Am. Chem. Soc.* **1997**, *119*, 10430. Martin, J. M. L.; Aviyente, V.; Lifshitz, C. *J. Phys. Chem. A* **1997**, *101*, 2597. Hirao, K.; Yamabe, S.; Sano, M. *J. Phys. Chem.* **1982**, *86*, 2626. Mayer, P. M. *J. Phys. Chem. A* **1999**, *103*, 5905. Delbene, J. E. *J. Am. Chem. Soc.* **1993**, *115*, 1610. Mestdagh, J. M.; Binet, A.; Sublemontier, O. *J. Phys. Chem.* **1989**, *93*, 8300. Hirao, K.; Yamabe, S.; Sano, M. *J. Phys. Chem.* **1982**, *86*, 2626. Meotner, M. *J. Am. Chem. Soc.* **1978**, *100*, 4694. (d) $H^+(CH_3OH)_{2,3}$: Hirao, K.; Sano, M.; Yamabe, S. *Chem. Phys. Lett.* **1982**, *87*, 181. Xia, P.; Hall, M.; Furlani, T. R.; Garvey, J. F. *J. Phys. Chem.* **1996**, *100*, 12235. Pardo, L.; Mazurek, A. P.; Osman, R. *Int. J. Quantum Chem.* **1990**, *37*, 701. Hillenbrand, E. A.; Scheiner, S. *J. Am. Chem. Soc.* **1984**, *106*, 6266. Hirao, K.; Sano, M.; Yamabe, S. *Chem. Phys. Lett.* **1982**, *87*, 181. Chang, H. C.; Jiang, J. C.; Chang, H. C.; Wang, L. R.; Lee, Y. T. *Isr. J. Chem.* **1999**, *39*, 231. Lee, S. Y.; Shin, D. N.; Cho, S. G.; Jung, K. H.; Jung, K. W. *J. Mass Spectrom.* **1995**, *30*, 969. (e) $H^+(CH_3CH_2OH)_2$: Xie, Z.; Manning, J.; Reed, R. W.; Mathur, R.; Boyd, P. D. W.; Benesi, A.; Reed, C. A. *J. Am. Chem. Soc.* **1996**, *118*, 2922. Mestdagh, J. M.; Binet, A.; Sublemontier, O. *J. Phys. Chem.* 1989, *93*, 8300. (f) $Cl^- H_2O$: Richardson, S. L.; Francisco, J. S.; Mebel, A. M.; Morokuma, K. *Chem. Phys. Lett.* **1997**, *270*, 395. Latajka, Z. *J. Mol. Struct.* (*Theochem*) **1992**, *85*, 225. (g) $NO_3 \cdot (HNO_3)_{1,2}$: Wlodek, S.; Luczynski, Z.; Wincel, H. *Int. J. Mass Spectrom. Ion Processes* **1980**, *35*, 39.
(20) Tholmann, D.; Tonner, D. S.; McMahon, T. B. *J. Phys. Chem.* **1994**, *98*, 2002.
(21) Grimsrud, E. P.; Kebarle, P. *J. Am. Chem. Soc.* **1973**, *95*, 7939.
(22) Beauchamp, J. L.; Caserio, M. C. *J. Am. Chem. Soc.* **1972**, *94*, 2638.
(23) Tardy, D. C.; Rabinovitch, B. S. *Chem. Rev.* **1977**, *77*, 370.
(24) Brown, T. C.; Taylor, J. A.; King, K. D.; Gilbert, R. G. *J. Phys. Chem.* **1983**, *87*, 5214.

(25) Krongauz, V. V.; Rabinovitch, B. S. *J. Chem. Phys.* **1983**, *78*, 3872.
(26) Davidson, J. A.; Fehsenfeld, F. C.; Howard, C. J. *Int. J. Chem. Kinet.* **1977**, *9*, 17.
(27) Yamdagni, R.; Kebarle, P. *J. Am. Chem. Soc.* **1971**, *93*, 7139.
(28) Pilling, M. J., Smith, I. W. M., Ed. *Modern Gas Kinetics, Theory, Experiment, and Application*; Blackwell Scientific Publications: Oxford, 1987; Chapter A4.
(29) Su, T.; Chesnavich, W. J. *J. Chem. Phys.* **1982**, *76*, 51.
(30) Tardy, D. C.; Rabinovitch, B. S. *Chem. Rev.* **1977**, *77*, 370.
(31) Chase, M. W., Jr.; Davies, C. A.; Downey, J. R., Jr.; Frurip, D. J.; McDonald, R. A.; Syverud, A. N. JANAF Thermochemical Tables. *J. Phys. Chem. Ref. Data Suppl. 1* **1985**, 14.
(32) Meot-ner, M.; Speller, C. V. *J. Phys. Chem.* **1986**, *90*, 6616.
(33) Cunningham, A. J.; Payzant, J. D.; Kebarle, P. *J. Am. Chem. Soc.* **1972**, *94*, 7672.
(34) Dalleska, N. F.; Honma, K.; Armentrout, P. B. *J. Am. Chem. Soc.* **1993**, *115*, 12125.
(35) Honma, K.; Sunderlin, L. S.; Armentrout, P. B. *J. Chem. Phys.* **1993**, *99*, 1623.
(36) Meot-ner, M.; Field, F. H. *J. Am. Chem. Soc.* **1977**, *99*, 998.
(37) Honma, K.; Sunderlin, L. S.; Armentrout, P. B. *Int. J. Mass Spectrom. Ion Processes* **1992**, *117*, 237.
(38) Lau, Y. K.; Ikuta, S.; Kebarle, P. *J. Am. Chem. Soc.* **1982**, *104*, 1462.
(39) Hiraoka, K.; Takimoto, H.; Yamabe, S. *J. Phys. Chem.* **1986**, *90*, 5910.
(40) Grimsrud, E. P.; Kebarle, P. *J. Am. Chem. Soc.* **1973**, *95*, 7939.
(41) Larson, J. W.; McMahon, T. B. *J. Am. Chem. Soc.* **1982**, *104*, 6255.
(42) Bomse, P. S.; Beauchamp, J. L. *J. Phys. Chem.* **1981**, *85*, 488.
(43) Meot-ner, M. *J. Am. Chem. Soc.* **1978**, *100*, 4694.
(44) Lau, Y. K.; Saluja, P. P. S.; Kebarle, P. *J. Am. Chem. Soc.* **1980**, *102*, 7429.
(45) Davidson, J. A.; Fehsenfeld, F. C.; Howard, C. J. *Int. J. Chem. Kinet.* **1977**, *9*, 17.
(46) Lee, N.; Keesee, R. G.; Castleman, A. W., Jr. *J. Chem. Phys.* **1980**, *72*, 1089.
(47) Wlodek, S.; Luczynski, Z.; Wincel, H. *Int. J. Mass Spectrom. Ion Phys.* **1980**, *35*, 39.
(48) Hiroaka, K.; Mizuse, S.; Yamabe, S. *J. Phys. Chem.* **1988**, *92*, 3943.
(49) Arshadi, M.; Yamdagni, R.; Kebarle, P. *J. Phys. Chem.* **1970**, *74*, 1475.
(50) Sieck, L. W. *J. Phys. Chem.* **1985**, *89*, 5552.
(51) Yamabe, S.; Furumiya, Y.; Hiraoka, K.; Morise, K. *Chem Phys. Lett.* **1986**, *131*, 261.
(52) Larson, J. W.; McMahon, T. B. *J. Am. Chem. Soc.* **1984**, *106*, 517.